FACTA UNIVERSITATIS
Series: **Electronics and Energetics** Vol. 32, N^{o} 2, June 2019, pp. 287-302
https://doi.org/10.2298/FUEE1902287S

PREDICTION OF THE EM SIGNAL DELAY IN THE IONOSPHERE USING NEURAL MODEL

Zoran Stanković, Nebojša Dončov

University of Niš, Faculty of Electronic Engineering

Abstract. *Neural model capable to accurately and efficiently predict a propagation delay of electromagnetic signal in the ionosphere is proposed in this paper. The model performs this prediction for a given geographic location in Europe between 40° (N) and 70° (N) latitude and 10° (W) and 30° (E) longitude, according to the following parameters: particular day in a year, time during the day and frequency of a signal carrier. Architecture of the model consists of four multilayer perceptron (MLP) networks with the task to estimate, for the known values of the previously mentioned input parameters of the model, the approximate value of free ions concentration in the atmosphere along the signal propagation path above the geographic location of the receiver. Based on the estimated ions concentration and taking into account the considered frequency of the signal carrier, the model calculates the time delay of signal propagation in the ionosphere. The developed neural model is applicable on the whole territory of Republic of Serbia, for all four weather seasons in the period of low solar activity. The results of using the proposed model for the prediction of time delay of the GPS (Global Positioning System) signal in the area of city of Niš are provided in the paper.*

Key words: *neural networks, neural model, ionosphere, total electron content, signal delay estimation, global positioning system*

1. INTRODUCTION

Concentration of ions is much higher in the ionosphere than in any other atmosphere layer and, as a result, the parameters of the electromagnetic (EM) signals propagating throughout the ionosphere can be significantly affected [1-4]. Signals of modern satellite communication systems such as satellite positioning systems, navigation systems, broadcasting systems, time service systems and remote sensing systems, propagate partially through the ionosphere. Following changes in the propagating signals of these systems can appear: the change of trajectory and time delay of the signal, modification of the frequency of the signal, variation in the phase of signal carrier and change in the

Received October 28, 2018; received in revised form December 12, 2018
Corresponding author: Zoran Stanković
University of Nis, Faculty of Electronic Engineering, Aleksandra Medvedeva 14, 18000 Niš, Serbia
(E-mail: zoran.stankovic@elfak.ni.ac.rs)

signal polarization [1,3]. These changes may influence the proper operation of the aforementioned wireless systems, and the space-time characterization of these changes can be of great importance for their design and exploitation.

Typical examples of how these changes of signal parameters due to its propagation in the ionosphere have a negative impact on an operation of satellite systems are: the variation of signal propagation delay introduces the error in the determination of the user position on Earth using satellite navigation systems (e.g. using GPS), the change in frequency due to the additional Doppler effect in the ionosphere interrupts the correct operation of Synthetic-Aperture Radar (SAR) system, the Faraday rotation of wave propagation and the change of the wave shape of the EM signal interrupts the correct work of broadcasting satellites, etc. [2,3].

Ions concentration in the ionosphere as well as the distribution of this concentration with the altitude (so-called height profile of the ionosphere) contribute strongly to the changes of previously mentioned signal characteristics while propagating through the ionosphere [1,3]. Therefore, for the description and prediction of previously mentioned changes of satellite signals parameters in the ionosphere, it is of very high importance to know the distribution of ions concentration along the path of the signal propagation through the ionosphere which is represented by the Total Electron Content (TEC) values [1,3-8]. TEC is the total number of electrons integrated between two points, along a tube of one meter squared cross section which surrounds the path of the signal through the ionosphere. The distribution of free ions concentration in the ionosphere, and therefore the TEC value, depend on a number of spatial and time parameters, among them the most important are: the geographic location of the location above which the height profile of the ionosphere is observed, the current weather season, the time during the day and intensity of Sun activity within the 11-years solar cycle [1,3-8].

A possibility to replace the complex and slow approaches of determining the TEC values based on classical vertical ionosphere sounding [1,3] arises with an introduction of a system for global positioning. New methods appear capable to determine the current value of TEC value in the vertical height profile of the ionosphere above the receiver position, by using GPS receiver and receiving signal at two different frequencies. For this purpose, the Ionospheric Monitoring and Prediction Center (IMPC) [6] is very important today and it uses more than 160 Global Navigation Satellite System (GNSS) receivers for real-time TEC measurements, placed all around the world. However, for the design and analysis of the operation of satellite communication systems, it is of greater importance to know the variation and prediction of TEC values in a longer period of time (so-called TEC forecasting) above some specific geographic location rather than obtaining the current TEC value above a number of geographic locations that are defined and conditioned by the distribution of measurement equipment. Therefore, the development of model for the TEC forecasting is in the focus of today's research. Performing the greater number of measurements in a longer period of time for specific locations within some monitored geographic area and applying the classification of measured results by using the statistical analysis and mathematical interpolation methods, it is possible to develop an empirical model of the ionosphere for given geographic area that can perform the prediction of TEC values for a specific moment in time and desired location inside the considered area [3,4,7,8]. This approach was demonstrated in [7] with the development of

TEC forecasting model that uses the Kriging interpolation technique and also in [8] where such model was developed by using the spherical harmonic expansion approach.

Alternative approach for the development of the TEC forecasting model is based on using the artificial neural networks (ANNs) to design the model of ionosphere and to predict the TEC values. This approach offers a much simpler development of ionosphere model and its easier implementation than empirical model based on statistical methods and complex mathematical interpolations. Once successfully trained, the neural model avoids, during the exploitation, a manipulation with a large number of measurement data organized as tables, graphics or the matrix database. Therefore, for the given values of input parameters related to the spatial-time location of receiving terminal, the neural model is capable to predict the TEC value in the vertical profile of the ionosphere in a very short time interval. In addition to that, thanks to its powerful interpolation and generalization capabilities, the neural model provides a better accuracy prediction of TEC value in comparison with the classical statistical models in geographic areas with a sparse distribution of probe stations in the ionosphere. The mentioned characteristics of ANNs for the modelling of the ionosphere and prediction of TEC values were demonstrated in [12-18]. In [12] a regional TEC model based on ANN has been designed and tested using data sets collected by the Brazilian GPS network covering periods of low and high solar activity. In [13] a local specific neural model was proposed for the prediction of TEC values above the area in Iran based on MultiLayer Perceptron (MLP) network. Performances of that model were compared with the polynomial fitting and Kriging interpolation. Local specific wavelet neural model (WNN) for TEC prediction over Azerbaijan was given in [14]. In [15] a neural model for TEC value prediction in the vertical profile of ionosphere above the city Parit Raja, Johor in Malaysia was presented for low to medium solar activity period. In [16] and [17] regional neural models based on MLP networks were suggested to predict the TEC values and to perform the calculation of the time delay [16] and the carrier phase advance [17] of the EM signal in the ionosphere above the Mediterranean area. Regional neural model for the prediction of TEC values above the China, realized by using genetic algorithm-based neural network (GA-NN) and measured TEC values from 43 permanent GPS stations in China was shown in [18].

This paper represents the continuation of the research conducted in [16,17]. By modifying the approach in the design of neural model and with further development of the neural model architecture from [16,17] and use of the new set of samples in the neural model training that covers the territory of the Republic of Serbia, the new neural model is here developed and proposed. It performs the prediction of TEC value and calculation of time delay of EM signal propagating in the ionosphere for the whole territory of the Republic of Serbia and for the all four weather seasons in the period of low solar activity. Under the assumption of the low solar activity it is considered the activity of Sun with average monthly values below 80 SRFU (10.7 cm solar radio flux ($F_{10.7}$) units that roughly lasts around 4 years and it is repeating every 11 years in average [5].

2. Neural Model of the Ionospheric Time Delay of the EM signal

For the development of the proposed neural model we use data of measured TEC values provided in [4]. Most of measured results from [4] were obtained by probe stations in the ionosphere in order to provide the map of TEC values distribution above the areas

that cover the significant part of Europe and Mediterranean. Regarding the area of Europe, the measurement of current TEC values was performed during the period of 27 months. Authors of this paper were directed to use the measured results from [4] due to the following reasons. During the neural model development, the new period of low solar activity has not yet started and therefore the acquisition of data by IMPC server within a period of minimum one year would be possible only in the coming period. Alternative was to use a database of measured results for low solar activity periods older than 11 years. The only database that covers solar minima with a duration longer than 1 year, whose measured results can be considered valid for the territory of the Republic of Serbia and it was available to the authors of this paper during the model development is the database given in [4]. Measured values were classified by geographic regions and measured $F_{10.7}$ solar flux and averaged for all four weather seasons. During the measurements it was noticed that TEC value depended on the geographic location for which the height profile of atmosphere was monitored, current weather season and the time interval during the day as well as intensity of solar flux directly connected with the actual period of solar activity. In addition, it was observed that for the locations lying on the same latitude and for the measurements taken on same day and exact time during that day, the approximately same values of TEC were measured. Therefore, the change of TEC values with longitude could be incorporated into a variation of TEC with a local time. On the other side, it was shown in [3] that the time delay of signal depended on TEC values along the propagation path throughout ionosphere and frequency of the carrier.

Taking this into account, the proposed neural model of the ionospheric time delay of the EM signal has on its input the following variables: date in short format (dd-mm) defining the day and month and based on which the appropriate season is selected, latitude of receiver station (l_a), time during 24 hours of local time (h) and frequency of the carrier (f). Neural model is developed for the period of low solar activity where fluctuation of solar flux is not significant, therefore the dependence of TEC value with a variation of solar flux is not considered here. For the development of neural Ionospheric Time Delay (ITD) model, MLP network is used so the shortened name of the model is MLP_ITD.

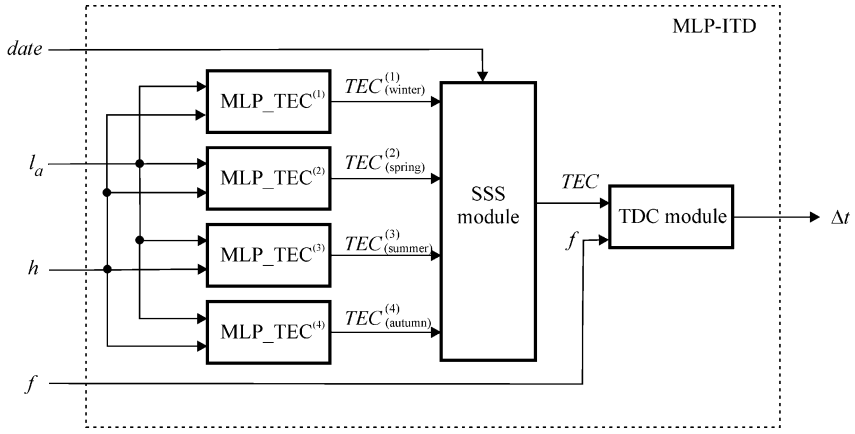

Fig. 1 Architecture of the ionospheric time delay neural model (MLP_ITD model)

Architecture of MLP_ITD model is shown in Fig. 1. The model consists of four MLP_TEC$^{(s)}$ modules (where s=1,2,3,4; each module corresponds to one season during the year), season selection and smoothing (SSS) module and time delay calculation (TDC) module.

Each of MLP_TEC$^{(s)}$ modules has a task to predict the TEC value in the vertical profile of ionosphere above the receiver for the specific season, the latitude of the receiver (l_a) and moment in time (h). Therefore, the transfer function of s-th module is of the form $TEC^{(s)}=f_{\mathrm{MLP\_TEC}(s)}(la,h)$. SSS module based on the *date* value selects the corresponding outputs of the MLP_TEC$^{(s)}$ networks, uses these values to form the final TEC value and forward it to the module that is responsible to find the time delay in the ionosphere (TDC module). TDC module, for chosen TEC value and frequency of the carrier, calculates the time delay as:

$$\Delta t = f_{TDC}(TEC, f) = \frac{40.3}{cf^2} \cdot TEC \tag{1}$$

where the value of TEC is expressed in units 10^{16} electron/m^2, c is a speed of light in m/sec and f is a frequency of the signal is Hz. In line with this, the processing function of TEC_ITD model can be expressed as:

$$\Delta t = f_{MLP\_ITD}(s, l_a, h, f) = f_{TDC}(f_{MLP\_TEC(s)}(l_a, h), f) \tag{2}$$

2.1. Architecture of the MLP_TEC$^{(s)}$ module

For the realization of each MLP_TEC$^{(s)}$ module, MLP network with one hidden layer is used (Fig. 2). The input layer of neurons is a buffer layer for a vector of input variables $\mathbf{x} = [l_a\ h]$, so it has only two neurons: i_1 and i_2. The hidden layer has a variable number of neurons n_1, n_2,...n_H, where H is a number of hidden neurons. The output layer has only one neuron o_1 which on its output gives the value of TEC. Outputs of each input neuron are forwarded to the input of each neuron in the hidden layer multiplied with a corresponding connection weight factor. Also, the outputs of all hidden neurons are sent to the input of neuron in the output layer, again multiplied with corresponding connection weight factor.

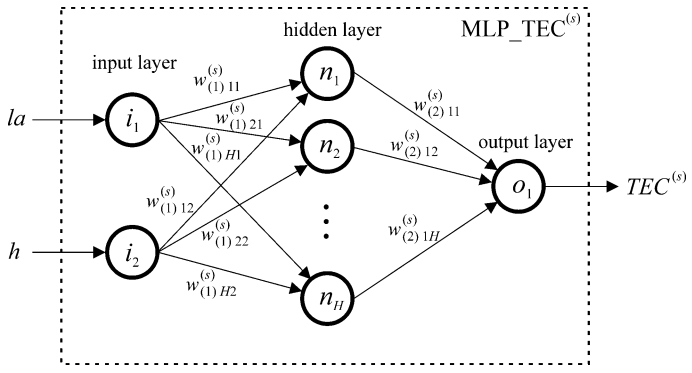

Fig. 2 Architecture of the MLP_TEC$^{(s)}$ module

For all neurons in the hidden layer, the hyperbolic tangent sigmoid transfer function is chosen as the activation function of neurons:

$$F(u)=\frac{e^{u}-e^{-u}}{e^{u}+e^{-u}} \tag{3}$$

so that the processing function of MLP network and therefore of MLP_TEC$^{(s)}$ module is of the form:

$$TEC^{(s)} = f_{MLP\_TEC(s)}(l_a, h) = \mathbf{w}_{(2)}^{(s)} F(\mathbf{w}_{(1)}^{(s)}\mathbf{x}+\mathbf{b}_{(1)}^{(s)})+\mathbf{b}_{(2)}^{(s)} \tag{4}$$

where input weight matrix is $\mathbf{w}_{(1)}{}^{(s)}=[w_{ij(1)}{}^{(s)}]_{H\times 2}$, layer weight matrix is $\mathbf{w}_{(2)}{}^{(s)}=[w_{ij(2)}{}^{(s)}]_{1\times H}$ input bias vector is $\mathbf{b}_{(1)}{}^{(s)}=[b_{i(1)}{}^{(s)}]_{H\times 1}$ and output bias vector $\mathbf{b}_{(2)}{}^{(s)}=[b_{i(2)}{}^{(s)}]_{1\times 1}$. Element $w_{ij(1)}{}^{(s)}$ represents the weight of the connection between *j*-th neuron of input layer and *i*-th hidden neuron, $w_{ij(2)}{}^{(s)}$ represents the weight of the connection between *j*-th neuron of hidden layer and *i*-th output neuron, $b_{i(1)}{}^{(s)}$ is bias of the *i*-th hidden neuron and $b_{i(2)}{}^{(s)}$ is bias of the *i*-th output neuron. The general notation for the architecture of MLP network, which has one hidden layer with *H* neurons in total, is MLP-*H*, and for the network chosen to select the value of TEC for *s*-th season and incorporated into the MLP_TEC$^{(s)}$ module is MLP_TEC$^{(s)}$: MLP-*H*.

2.2. Architecture of the SSS module

SSS module has a task to identify the current season based on particular day in the month (expressed as dd-mm input), choose appropriate outputs from the MLP_TEC$^{(s)}$ networks and form final TEC value (Fig. 1) At the same time this module provides smooth transitions between neighbouring seasons and avoids the rapid changes of TEC values through switching of MLP_TEC$^{(s)}$ networks (Fig. 3). Transition area between two neighbouring seasons contains 30 days (the last 15 days of the previous season and the first 15 days of the next season). In this transition area a linear smoothing scheme is applied by using the algorithm shown in Fig. 3.

3. TRAINING AND TESTING OF THE MLP_ITD MODEL

For the training and testing of MLP_ITD model, we used data from [4] which are measured TEC values in the ionosphere above the part of Europe, 40°(N)-70°(N) latitude, 10°(W)-30°(E) longitude, so that they basically include the territory of the Republic of Serbia. Training and testing of MLP_ITD module represent separate and independent training of MLP network for each MLP_TEC$^{(s)}$ module. In order to generate the sets for MLP networks training and testing, the measured results of TEC values in the period of one year with a low solar activity, with an average solar activity of 75 SRFU, were chosen. These results are shown on four plots with TEC iso-contours (Fig 4a-4.d) [4]. Each plot shows the dependence of TEC value with the location above which the height profile of ionosphere is observed and with local time for an appropriate season (Fig 4.a for winter, Fig 4.b for spring, Fig 4.c for summer and Fig 4.d for autumn). For each season, the training and test sets were generated by sampling from the plot corresponding to that season. For *s*-th season, the set for the training of neural network is a set of triplets

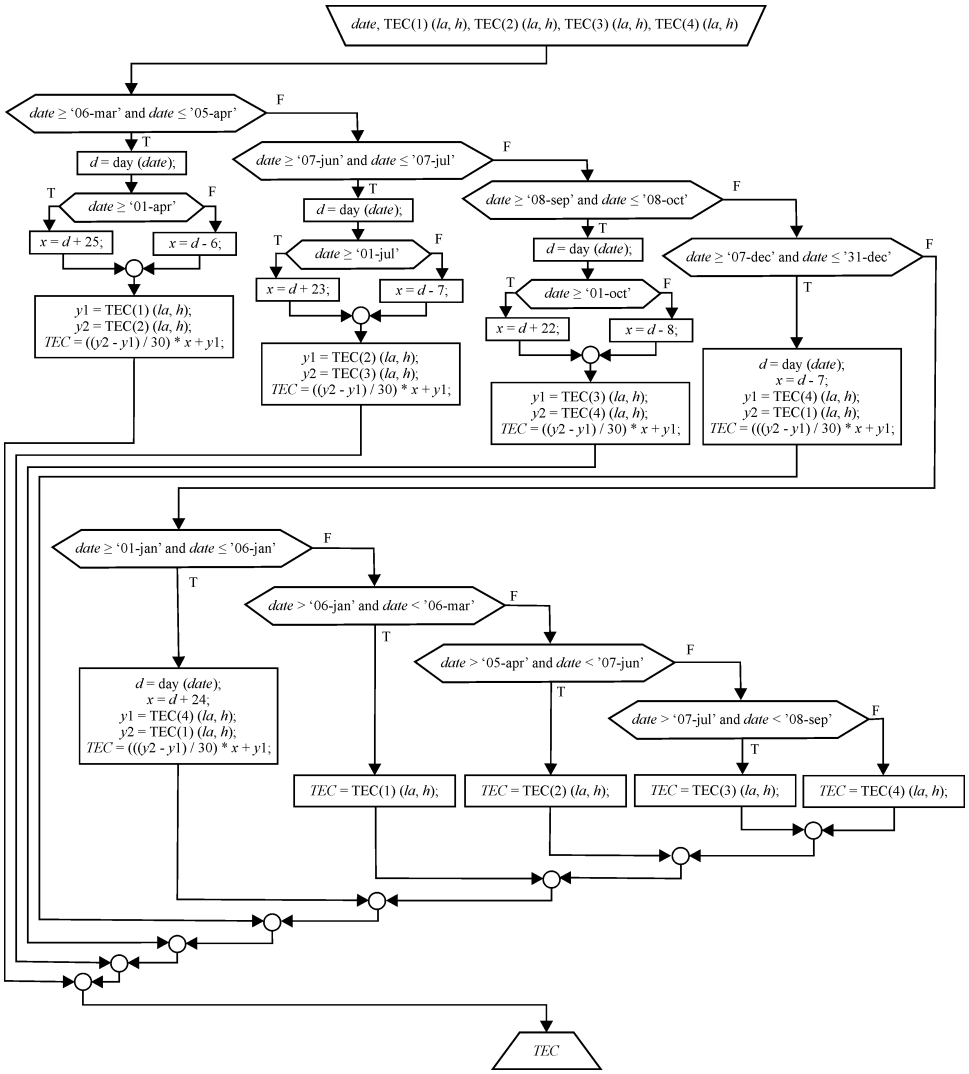

Fig. 3 Season selection algorithm with smoothing scheme at the boundaries of the MLP_TEC$^{(s)}$ networks used in the SSS (Season Selection and Smoothing) module

with a form $\mathcal{L}_s=\{(la_i,h_i,TEC_{(ref)i}^{(s)}) \mid i=1,...L_s\}$, where $TEC_{(ref)i}^{(s)}$ represents the target value of neural network output for i-th combination of input variables la_i,h_i while L_s is a total number of training samples of network for s-th season. Similarly, for s-the season the training set of the neural network is a set of triplets of the form $\mathcal{T}_s=\{(la_i^t,h_i^t,TEC_{(ref)i}^{t\,(s)}) \mid i=1,...T_s\}$, where index t in superscript means that these values are for testing and not for training, while T_s is a number of test samples for s-th season. Each triplet for training and testing represents the coordinates of the point on iso-contour plot. Training set was

generated by sampling these points from the TEC iso-contour plots for the values of latitude l_a = 40°,45°,50°,55°,60°,65°,70°, while the testing set was obtained by sampling

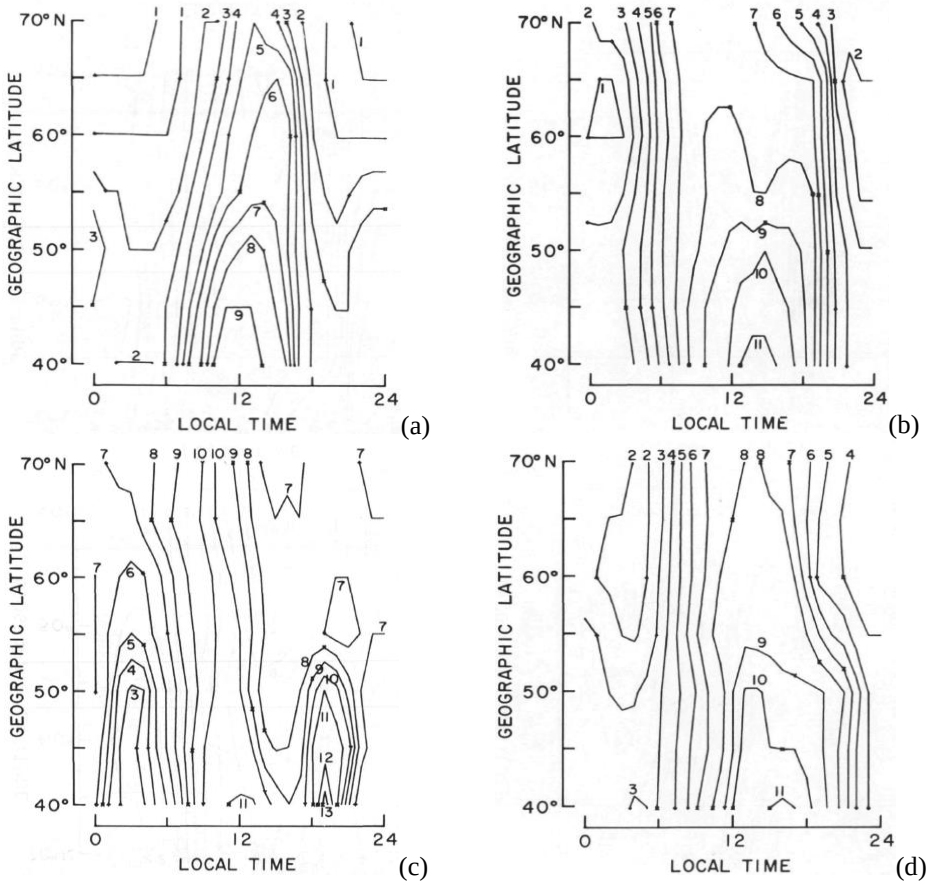

Fig. 4 Contour plots of measured TEC data vs. hours and latitude for (a) winter, (b) spring, (c) summer and (d) autumn (TEC units are in10^{16} electron/m^2). Measurements were performed in a period of low solar activity where the average solar activity was 75 SRFU [4].

these points from the TEC iso-contours for the values of latitude *la* = 43.4°, 52.5°, 62.5°. As a result, the training and testing sets with the following distribution of total number of samples by seasons: L_1= 109, L_2= 117, L_3= 132, L_4= 112 and T_1= 46, T_2= 52, T_3= 52 and T_4= 45 were generated.

The main goal of MLP network training for each MLP_TEC$^{(s)}$ module is to adjust the values of connection weight matrices $\mathbf{w}_{(1)}^{(s)}$ and $\mathbf{w}_{(2)}^{(s)}$, and bias matrices $\mathbf{b}_{(1)}^{(s)}$ and $\mathbf{b}_{(2)}^{(s)}$ so that the mean square error of network output $TEC_i^{(s)}$ with respect to the target value $TEC_{(ref)i}^{(s)}$, observed on the whole training set, is equal or lower from the specified maximum training error E_t:

$$\frac{1}{L_s}\sum_{i=1}^{L_s}((TEC_i^{(s)})^2-(TEC_{(ref)i}^{(s)})^2)\le E_t \tag{5}$$

The model was realized in the MATLAB environment and the Levenberg-Marquartd training method was used with a given targeted maximum training error $E_t=10^{-4}$.

In order to quantify the success of the training of each MLP_TEC$^{(s)}$ network and its generalization abilities, the testing of training networks was conducted on test sets and the following criteria were considered: the worst case error (*WCE*) value

$$WCE^{(s)}=\frac{\max\limits_{i=1,..,Ts}\left(\left|TEC_i^{t(s)}-TEC_{(ref)i}^{t(s)}\right|\right)}{\left|\max\limits_{i=1,..,Ts}(TEC_{(ref)i}^{t(s)})-\min\limits_{i=1,..,Ts}(TEC_{(ref)i}^{t(s)})\right|} \tag{6}$$

where $TEC_i^{t(s)}$ is an output of MLP_TEC$^{(s)}$ network on *i*-th sample, the average test error (*ATE*) value:

$$ATE^{(s)}=\frac{\sum\limits_{i=1}^{T_s}\left|TEC_i^{t(s)}-TEC_{(ref)i}^{t(s)}\right|}{T_s\left|\max\limits_{i=1,..,Ts}(TEC_{(ref)i}^{t(s)})-\min\limits_{i=1,..,Ts}(TEC_{(ref)i}^{t(s)})\right|} \tag{7}$$

and the Pearson product-moment correlation value (r^{PPM})

$$r^{PPM\,(s)}=\frac{\sum\limits_{i=1}^{T_s}(TEC_{(ref)i}^{t(s)}-\overline{TEC}_{ref}^{t(s)})(TEC_i^{t(s)}-\overline{TEC}^{t(s)})}{\sqrt{\sum\limits_{i=1}^{T_s}(TEC_{(ref)i}^{t(s)}-\overline{TEC}_{ref}^{t(s)})^2}\sqrt{\sum\limits_{i=1}^{T_s}(TEC_i^{t(s)}-\overline{TEC}^{t(s)})^2}} \tag{8}$$

where approapriate average values of referent TEC values of test set and average value of TEC values representing the output of MLP_TEC$^{(s)}$ network on test set are defined as:

$$\overline{TEC}_{ref}^{t(s)}=\frac{1}{T_s}\sum_{i=1}^{T_s}TEC_{(ref)i}^{t(s)}\quad \overline{TEC}^{t(s)}=\frac{1}{T_s}\sum_{i=1}^{T_s}TEC_i^{t(s)} \tag{9}$$

With the goal to obtain MLP_TEC$^{(1)}$ module with an accuracy as higher as possible for each season, the training and testing of different MLP-*H* networks ($2\le H\le 20$) were conducted.

3.1. Training and testing results of the MLP_TEC$^{(1)}$ networks (case *s*=1, winter)

Testing results for six MLP networks, trained and tested for the case *s*=1 (winter), with the highest r^{PPM} value are shown in Table 1.

MLP-8 network is chosen to be implemented into the MLP_TEC$^{(1)}$ module. Scattering diagram for the MLP_TEC$^{(1)}$:MLP-8 network on test set is shown in Fig. 5, where a good agreement between the TEC values, provided by MLP network, and the referent values

can be observed. The weight and biases values of the MLP TEC$^{(1)}$:MLP-8 network, obtained after training, are given in Table 2.

Table 1 Testing results for six MLP networks with the highest r^{PPM} value (MLP_TEC$^{(1)}$, winter)

MLP net	WCE [%]	ACE [%]	r^{PPM}
MLP-8	8.36	2.44	0.9948
MLP-14	6.38	2.78	0.9948
MLP-6	7.70	2.65	0.9935
MLP-9	8.34	2.59	0.9933
MLP-13	7.81	3.06	0.9929
MLP-5	9.33	3.01	0.9917

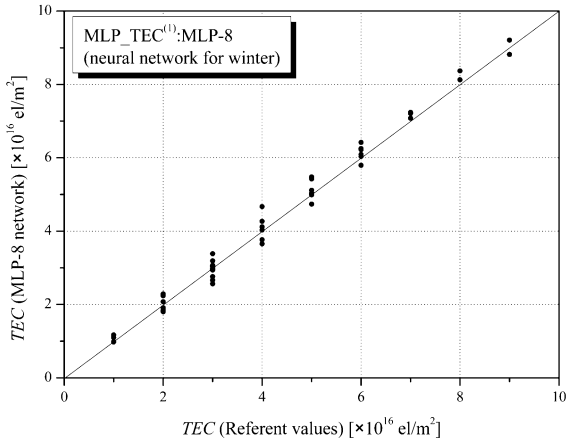

Fig. 5 Scattering diagram for MLP_TEC$^{(1)}$:MLP-8 network (winter, test set)

Table 2 Weight and bias values of the MLP_TEC$^{(1)}$:MLP-8 network

Input layer - Hidden layer connection		Hidden layer – Output layer connection	
$\mathbf{w}_{(1)}^{(1)} = \begin{bmatrix} 3.1005 & 5.8083 \\ -0.0970 & 6.2129 \\ -1.4987 & 5.1442 \\ 1.4532 & -5.0526 \\ -1.6962 & -2.8569 \\ -2.8776 & -0.6086 \\ -3.0905 & -5.8590 \\ 1.7390 & 2.8087 \end{bmatrix}$	$\mathbf{b}_{(1)}^{(1)} = \begin{bmatrix} -5.1380 \\ -2.4021 \\ 1.0726 \\ -1.0473 \\ -3.8530 \\ -1.1506 \\ 5.1722 \\ 3.8328 \end{bmatrix}$	$\mathbf{w}_{(2)}^{(1)} = \begin{bmatrix} -20.1482 \\ -0.8133 \\ -20.4490 \\ -21.3616 \\ 15.9412 \\ 0.2092 \\ -20.0613 \\ 15.7952 \end{bmatrix}^T$	$\mathbf{b}_{(2)}^{(1)} = \begin{bmatrix} -0.6764 \end{bmatrix}$

3.2. Training and testing results of the MLP_TEC$^{(2)}$ networks (case *s*=2, spring)

Testing results for six MLP networks, trained and tested for the case *s*=2 (spring), with the highest r^{PPM} value are shown in Table 3. MLP-9 network is chosen to be implemented into the MLP_TEC$^{(2)}$ module.

Scattering diagram for the MLP_TEC$^{(2)}$:MLP-9 network on test set is shown in Fig. 6. Again, a good agreement between the TEC values, provided by MLP network, and the referent values can be observed The weight and biases values of the MLP TEC$^{(2)}$:MLP-9 network, obtained after training, are given in Table 4.

Table 3 Testing results for six MLP networks with the highest r^{PPM} value (MLP_TEC$^{(2)}$, spring)

MLP net	WCE [%]	ACE [%]	r^{PPM}
MLP-9	7.29	2.59	0.9940
MLP-7	7.93	2.58	0.9937
MLP-15	8.64	2.67	0.9937
MLP-13	8.32	2.38	0.9934
MLP-11	8.19	2.51	0.9933
MLP-4	7.70	2.71	0.9931

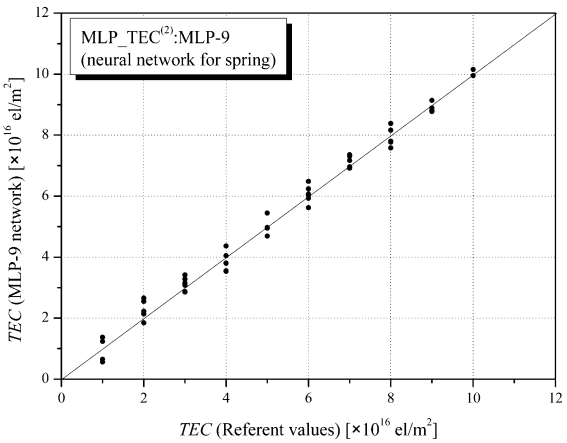

Fig. 6 Scattering diagram for MLP_TEC$^{(2)}$:MLP-9 network (spring, test set)

Table 4 Weight and bias values of the MLP_TEC$^{(2)}$:MLP-9 network

Input layer - Hidden layer connection

$$\mathbf{w}_{(1)}^{(2)} = \begin{bmatrix} 1.9519 & -0.6640 \\ -2.5718 & 0.1058 \\ 2.8918 & 4.4885 \\ -3.2473 & -11.3968 \\ 0.3306 & 5.5271 \\ -2.8642 & 8.0486 \\ -0.0907 & 6.6316 \\ -21.1541 & -0.5954 \\ -11.2798 & 25.7095 \end{bmatrix} \quad \mathbf{b}_{(1)}^{(2)} = \begin{bmatrix} -1.1567 \\ 1.6000 \\ -4.4849 \\ 1.9909 \\ 2.8569 \\ -2.3384 \\ -4.3630 \\ -20.8522 \\ -25.3295 \end{bmatrix}$$

Hidden layer – Output layer connection

$$\mathbf{w}_{(2)}^{(2)} = \begin{bmatrix} -0.7326 \\ -0.6468 \\ -0.2336 \\ 0.1585 \\ 0.5611 \\ 0.2608 \\ -0.7199 \\ -0.0391 \\ 0.0550 \end{bmatrix}^T \quad \mathbf{b}_{(2)}^{(2)} = \begin{bmatrix} -0.9077 \end{bmatrix}$$

3.3. Training and testing results of the MLP_TEC$^{(3)}$ networks (case *s*=3, summer)

As in previous two cases, in the case *s*=3 (summer), after the training, the testing of network on the test set corresponding to this season is performed. The testing results for six MLP networks with the highest r^{PPM} value, are given in Table 5 and, as a result, the MLP-12 network is selected to be used in the MLP_TEC$^{(3)}$ module. Scattering diagram for the MLP_TEC$^{(3)}$:MLP-13 network on test set is shown in Fig. 7.

TEC values provided by MLP network are very close to the referent values, as seen from Fig. 7. Table 6 contains the weight and biases values of the MLP_TEC$^{(3)}$:MLP-13 network.

Table 5 Testing results for six MLP networks with the highest r^{PPM} value (MLP_TEC$^{(3)}$, summer)

MLP net	WCE [%]	ACE [%]	r^{PPM}
MLP-13	8.90	3.12	0.9868
MLP-12	11.66	3.68	0.9835
MLP-9	19.62	3.49	0.9833
MLP-7	11.23	3.71	0.9832
MLP-8	11.35	4.08	0.9794
MLP-6	13.48	3.87	0.9781

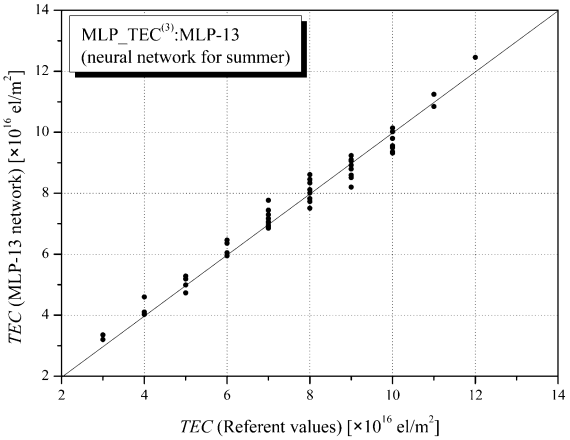

Fig. 7 Scattering diagram for MLP_TEC$^{(3)}$:MLP-13 network (summer, test set)

Table 6 Weight and bias values of the MLP_TEC$^{(3)}$:MLP-13 network

Input layer - Hidden layer connection		Hidden layer – Output layer connection	

$$\mathbf{w}_{(1)}^{(3)} = \begin{bmatrix} 1.1354 & -6.5274 \\ 0.1130 & -4.3269 \\ -18.3535 & 5.9238 \\ -0.9037 & -3.9723 \\ 6.0756 & 6.4545 \\ 0.8992 & 3.5630 \\ -0.8749 & -3.6046 \\ 0.9679 & -2.5763 \\ 12.7813 & -4.6531 \\ 0.7351 & -3.3586 \\ 0.1686 & -4.1528 \\ 0.2968 & -7.3582 \\ -16.1540 & -0.3792 \end{bmatrix} \quad \mathbf{b}_{(1)}^{(3)} = \begin{bmatrix} -6.5660 \\ 3.7168 \\ 11.3957 \\ -2.6444 \\ -2.5691 \\ -0.5072 \\ 0.5026 \\ -0.4384 \\ -0.0037 \\ 2.5669 \\ 3.5370 \\ -6.6910 \\ -18.8584 \end{bmatrix}$$

$$\mathbf{w}_{(2)}^{(3)} = \begin{bmatrix} -0.7055 \\ -31.1147 \\ -0.1264 \\ -0.4923 \\ -0.2004 \\ 34.5148 \\ 34.9119 \\ -0.7086 \\ 0.1641 \\ -4.1611 \\ 35.4423 \\ 0.9535 \\ -11.3856 \end{bmatrix}^T \quad \mathbf{b}_{(2)}^{(3)} = \begin{bmatrix} -11.8833 \end{bmatrix}$$

3.4. Training and testing results of the MLP_TEC$^{(4)}$ networks (case *s*=4, autumn)

The same testing and training procedures are conducted for the case *s*=4 (autumn). The testing results for six MLP networks with the highest r^{PPM} value, trained for this season, are presented in Table 7. For the implementation into the MLP_TEC$^{(4)}$ module, MLP-8 network is chosen. Scattering diagram for the MLP_TEC$^{(4)}$:MLP-8 network on test set (Fig. 8) shows a good agreement between the TEC values provided by MLP

network and the referent values. Table 8 contains the weight and biases values of the MLP_TEC$^{(4)}$:MLP-8 network.

Table 7 Testing results for six MLP networks with the highest r^{ppm} value (MLP_TEC$^{(4)}$, autumn)

MLP net	WCE [%]	ACE [%]	r^{PPM}
MLP-8	8.25	2.42	0.9945
MLP-10	15.95	2.62	0.9923
MLP-11	12.11	2.66	0.9920
MLP-9	11.52	2.73	0.9915
MLP-18	9.11	3.07	0.9905
MLP-5	8.79	3.20	0.9905

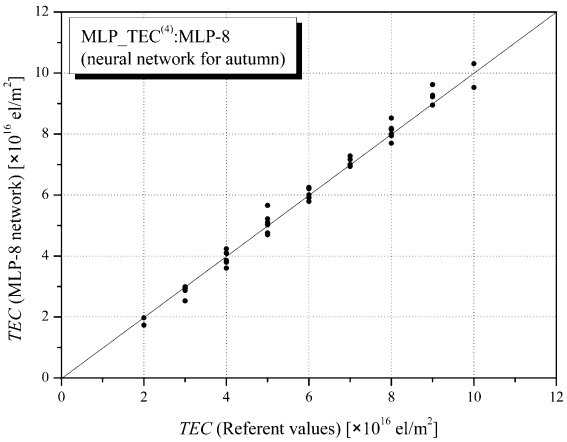

Fig. 8 Scattering diagram for MLP_TEC$^{(4)}$:MLP-8 network (autumn, test set)

Table 8 Weight and bias values of the MLP_TEC$^{(4)}$:MLP-8 network

Input layer - Hidden layer connection

$$\mathbf{w}_{(1)}^{(4)} = \begin{bmatrix} 1.7449 & -9.3968 \\ -0.2077 & -2.9541 \\ 0.8426 & 3.1785 \\ 4.9974 & -5.7140 \\ 3.0743 & 0.5274 \\ 6.0375 & 9.5886 \\ 6.6548 & 2.6519 \\ -2.5390 & 3.3781 \end{bmatrix} \quad \mathbf{b}_{(1)}^{(4)} = \begin{bmatrix} -9.0229 \\ -0.8679 \\ -2.0546 \\ -0.1558 \\ -0.1612 \\ 3.5531 \\ 4.9596 \\ -4.4276 \end{bmatrix}$$

Hidden layer – Output layer connection

$$\mathbf{w}_{(2)}^{(4)} = \begin{bmatrix} 0.3711 \\ -1.0730 \\ -0.6186 \\ 0.1555 \\ -0.3062 \\ 0.0939 \\ -0.2045 \\ -0.4360 \end{bmatrix}^T \quad \mathbf{b}_{(2)}^{(4)} = \begin{bmatrix} -0.7890 \end{bmatrix}$$

4. Simulation Results of the MLP_ITD Model In the Area of the City of Niš

MATLAB environment was used to realize, train and test MLP networks intended for the creation of the appropriate MLP_TEC$^{(s)}$ module. After that, in the same environment, we created MLP_TEC$^{(s)}$ modules together with the SSS module and the TDC module which, based on output of selected MLP_TEC$^{(s)}$ module, performs the time delay of the signal. As a final step the integration of all functional parts into the MLP_ITD model was done. This model is able to perform 24-hours prediction of the time delay of EM signal in the ionosphere for the period of low solar activity on the part of Europe that also covers the territory of the Republic of Serbia.

Proposed MLP_ITD model is used for the prediction of GPS signal delay above the area of the City of Niš caused by impact on the ionosphere on signal trajectory for the period of low solar activity. Signals on two frequencies belonging to the L-band and used by GPS service, f_1= 1575.42 MHz (L1) and f_2 = 1227.60 MHz (L2), are observed. Comparison of the results for the delay, obtained by prediction from the MLP_ITD model, and the referent values, obtained based on measured TEC values from [4], is shown in Figs. 9.a, Fig. 9.b, Fig. 9.c and Fig. 9.d for the cases when a day during which prediction is performed belongs to the winter, spring, summer and autumn (March 20, May 20, July 20 and November 20 respectively). A good agreement between results obtained by MLP_ITD model and referent values can be observed.

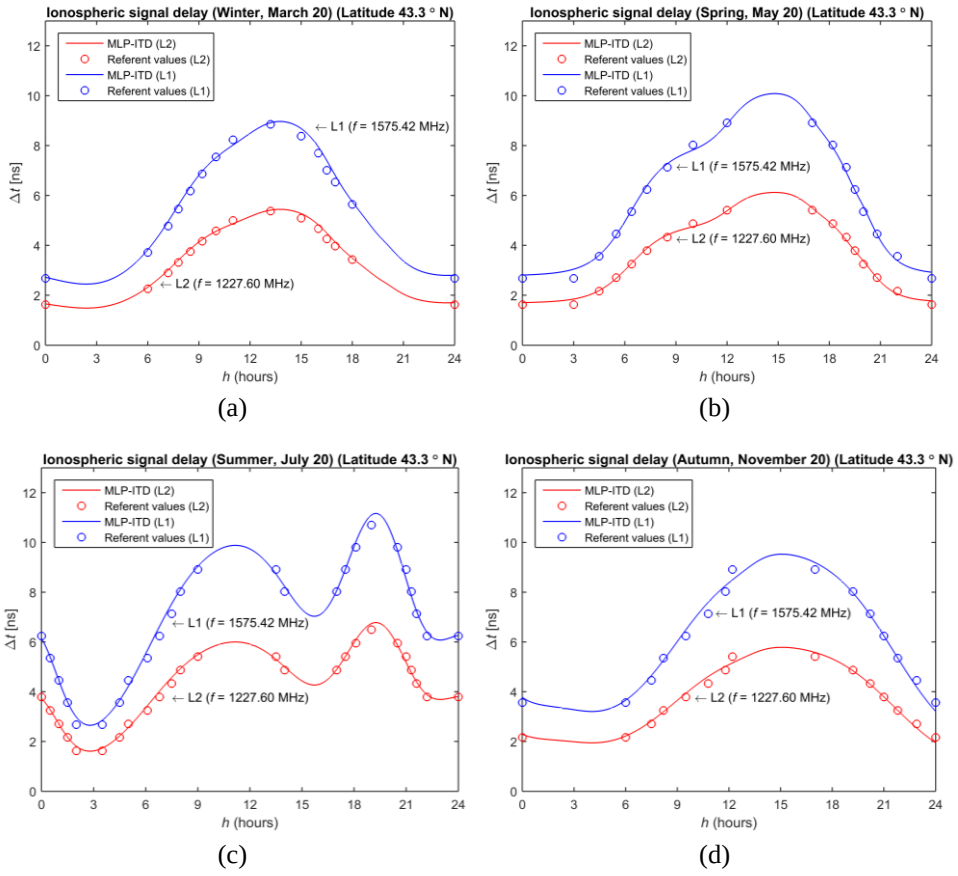

Fig. 9 Prediction of GPS signal delay obtained by using the MLP_ITD model on the territory of the city of Niš (latitude 43.3° N) during 24 h period and comparison of the estimated values with the referent values obtained by measurement for one day in (a) winter: March 20, (b) spring: May 20, (c) summer: July 20 and (d) autumn: November 20. Prediction is valid for the period of low solar activity.

4. CONCLUSION

Due to high concentration of ions, the ionosphere represents a specific EM medium that can change the signal characteristics of satellite communication systems that propagate through this atmospheric layer. One of the most significant changes, which affects the operation of these systems is a time delay of signal depending on current concentrations of free electrons (TEC) along the propagation path through the ionosphere. The current TEC value is a function of a number of parameters, among them the key parameters are: geographic location, local time, weather season and index of solar activity. This function is very complex and most researches are dedicated to the modelling of this dependence and prediction of TEC values. Due to parallel data processing and fast input-output propagation of signal, neural network modelling of TEC forecasting is in focus of today research. Neural models for TEC forecasting in the literature are of local specific nature and they can not be applied directly on the territory of the Republic of Serbia. In this paper, the neural model, based on MLP network, is proposed for an efficient prediction of TEC value and time delay of satellite signal in the ionosphere, applicable on the whole territory of the Republic of Serbia in the period of low solar activity. The results of using this model for the prediction of satellite signal delay in the area of the city of Niš, during 24 hours and for all four weather seasons, are in good agreement with the referent values obtained from measurements and therefore justify the researches regarding the application of MLP network for TEC forecasting.

Future researches will be directed towards further development and enhancement of architecture of MLP_ITD model aiming to achieve even better accuracy in prediction of TEC value and delay of satellite signal in the periods of low solar activity. Improvement of neural model accuracy will be conducted through:

- finer incorporation of TEC values variation within season depending of the day in year (achievable by including the day of year as additional input for the MLP_TEC networks).
- finer incorporation of longitudinal variation of TEC values that will take into account, besides local time effect as largest contributor to longitudinal variations, an interactions/coupling activities between the lower-middle-upper atmosphere layers, as well as the fact that the geomagnetic latitude lines are not parallel to the geographic latitude lines.

In order to collect data needed for the development of such enhanced TEC neural model, the acquisition of TEC values will be performed during 2019 by using the IMPC free service allowing to read the results of GNSS monitoring on a daily basis. This time interval is chosen as 2019 will be the first year that completely belongs to the period of low solar activity.

Acknowledgement: *This paper is supported by the project TR-32024 of the Ministry of Education, Science and Technological Development Education in the Republic of Serbia*.

REFERENCES

[1] M. Dragović, *Antene i prostiranje radio talasa*, Beopres, Beograd, 1996.

[2] T. Pratt, C. W. Bostian, J. E.Allnutt, *Satellite Communications*, John Wiley and Sons, 2003. god.

[3] S. Basu, J. Buchau, F.J. Rich, E.J. Weber, E.C. Field, J.L. Heckscher, P.A. Kossey, E.A. Lewis, B.S. Dandekar, L.F. McNamara, E.W. Cliver, G.H. Millman, J. Aarons, S. Basu, J.A. Klobuchar, S. Basu, M.F. Mendillo, *Ionospheric Radio Wave Propagation*, Chapter 10, pp. (10-1)–(10-111), 1985.

[4] J. A. Klobuchar and J. Aarons, *Numerical Models of Total Electron Content Over Europe and the Mediterranean and Multi-station Scintillation Comparisons*, INTERNATIONAL AGARD Agardograph, 1973.

[5] K. F. Tapping, "The 10.7 cm solar radio flux (F10.7)", *Space Weather*, vol. 11, pp. 394–406, 2013.

[6] Ionosphere Monitoring and Prediction Center (IMPC), Deutsches Zentrum für Luft- und Raumfahrt e.V. (DLR), German Aerospace Center, URL: http://impc.dlr.de/.

[7] R. Orus, M. Hernandez-Pajares, J.M. Juan and J. Sanz, "Improvement of global ionospheric VTEC maps by using kriging interpolation technique", *Journal of Atmospheric and Solar-Terrestrial Physics*, vol. 67, no. 16, pp. 1598–1609, 2005.

[8] B.K. Choi, W.K. Lee, S.K. Cho, J.U. Park and P.H. Park, "Global GPS Ionospheric Modelling Using Spherical Harmonic Expansion Approach", *Journal of Astronomy and Space Sciences*, vol. 27, no. 7, pp. 359–366, 2010.

[9] S. Haykin, *Neural Networks*, New York, IEEE, 1994.

[10] Q. J. Zhang, K. C. Gupta, *Neural Networks for RF and Microwave Design*, Artech House, 2000.

[11] C. Christodoulou, M. Georgiopoulos, *Applications of Neural Networks in Electromagnetics*, Artech House, 2001.

[12] R.F. Leandro, M.C. Santos, "A neural network approach for regional vertical total electron content modelling", *J. Studia Geophys. Geod.*, vol. 51, issue 2, pp. 279–292, 2007.

[13] M.R.G. Razin, B. Voosoghi and A. Mohammadzadeh, "Efficiency of artificial neural networks in map of total electron content over Iran", *Acta Geod. Geophys.*, issue 3, pp. 1–15, 2015.

[14] M.R.G. Razin, B. Voosoghi, "Wavelet neural networks using particle swarm optimization training in modeling regional ionospheric total electron content", *J. Atmos. Sol. Terr. Phys.*, vol. 149, pp. 21–30, 2016.

[15] M. J. Homam, "Prediction of Total Electron Content of the Ionosphere using Neural Network", *Jurnal Teknologi (Sciences & Engineering)*, vol. 78, no. 5–8, pp. 53–57, 2016.

[16] Z. Stanković, I. Milovanović, J. Jovanović, N. Dončov, B. Milovanović, "Estimation of the EM Wave Propagation Delay in the Ionosphere using Artificial Neural Networks", Presented at the YUINFO 2017 Conference, March 12-15, Kopaonik, Serbia, 2017, only a short abstract printed.

[17] Z. Stankovic, I. Milovanovic, N. Doncov, M. Sarevska and B. Milovanovic, "Estimation of the Carrier Phase Advance of the EM signal in the Ionosphere Using Neural Model", In Proceedings of the 52nd International Scientific Conference on Information, Communication and Energy Systems and Technologies, Niš, Serbia, June 28 - 30, 2017, pp. 211–215.

[18] R. Song, X. Zhang, C. Zhou, J. Liu and J. He, "Predicting TEC in China based on the neural networks optimized by genetic algorithm", *Advances in Space Research*, vol. 62, no. 4, pp. 745–759, 2018.